PHY 982 Homework 2

John Ash, Mengzhi Chen, Tong Li, Jason Surbrook

Feburary 27, 2018

1 Elastic scattering calculations of a nucleon on ^{208}Pb target

1.1 Coulomb scattering

In the case of point-Coulomb scattering, the Coulomb interaction between the projectile and the target with charges Z_1 and Z_2 is

$$V_c(R) = \frac{Z_1 Z_2 e^2}{R^2}, \tag{1}$$

where R is the distance between them. The Schrödinger's equation with this potential can be solved analytically. Related discussions are detailed in Ref.[1]. In sum, the angular distribution of point-Coulomb potential is described by the differential cross section

$$\sigma(\theta) = \frac{\eta^2}{4k^2 \sin^4(\theta/2)};\ \eta = \frac{Z_1 Z_2 e^2}{\hbar}\left(\frac{\mu}{2E}\right)^{\frac{1}{2}}, \tag{2}$$

where μ is the reduced mass and k is the wave number with the energy E. It worth noticing that the Eq. 6 is the same as the classical *Rutherford cross section.*

When the finite size of the target is included, due to different charge distributions, the interaction between the projectile and the target becomes more complicated. The case for uniform distribution over a sphere are formulated in Ref. [1].

Normally, these potentials are not analytically solvable. Sometimes, we can apply the *plane wave Born approximation* (PWBA) for the Coulomb scattering. Under PWBA, the differential cross section is

$$\sigma(\theta) = \frac{\eta^2}{4k^2 \sin^4(\theta/2)} \left|F(\theta)\right|^2, \tag{3}$$

where $F(\theta)$ is called the *form factor* related with the charge distribution as

$$F(\theta) = \int e^{i(\vec{k}_f - \vec{k}_i)\cdot\vec{r}'} \rho(r') d^3 r'. \tag{4}$$

In sum, we see the finite size of the target can give cross sections different from the point-like case.

1.2 The optical potential

In this section, we study the elastic scattering between nucleons and the ^{208}Pb target with the help of FRESCO[2] . Their effective interaction is referred to as the optical potential. We take the global parameterizations from Ref. [3, 4] as the input for FRESCO.

In the first step, we take two lab energies 5 and 50 (40) MeV for proton (neutron) in our calculations. The results together with experimental data are shown in Figure 1. It gives the angular distributions in center of mass for protons and neutrons. For the 5 MeV proton, the curve agrees well with the *Rutherford cross section*. Given that the radius parameter of optical potential is $r_w \sim 1.2\ fm$, we can estimate the Coulomb barrier for a proton to overcome. It should be

$$E_{Coul} \approx \frac{Z_1 Z_2 e^2}{r_w + R_2} \approx 15 \text{ MeV}. \tag{5}$$

We see that 5 Mev is much lower than the Coulomb barrier. Thus, this scattering can be referred as a point-like Coulomb scattering properly. The agreement with the *Rutherford cross section* also verifies this point. For neutrons, there is no Rutherford scattering cross section to compare against, hence the value of the neutron cross section being listed as fm^2. At 5 MeV the cross section hints at a broad diffraction pattern. Since 50 MeV is strong enough to overcome the Coulomb barrier, the effective interaction plays a role and induces a diffraction pattern in Figure 1. The neutron cross section at 40 Mev exhibits a similar behavior, speaking to the dominance of the nuclear interaction at this energy. We can also see that our curves basically obey same trends as experiments. However, they deviate in values, especially for neutron. It is because we use the global parameterizations. We will include the qualitative analyses and better fittings in the next section. In order to explore the influence of the optical potential, we will use $E_{lab} = 50$ MeV in following calculations.

In the next step, we would like to see the influences of the depth of optical potential's imaginary part of the S-matrix. Fixing other parameters, we scale the depth of imaginary parts V_i (including volume, surface derivative and spin-orbit potentials) a factor of 1.5, 0.5 and 0. The modules of S-matrix with for the proton and the neutron are shown in Table 1 and 2. We can see that as we lower the depth, $|\mathbf{S}|^2$ fluctuates and eventually converges to one which indicates an elastic scattering. It inspires us that the imaginary parts can describe absorptions in scattering processes. It also worth noticing the fluctuation of $|\mathbf{S}|^2$ with varying V_i in each partial wave. For this reason, there is no simple monotonous relations between the relative depth $\bar{V}$ and the total absorptive cross section.

Moreover, we are interested in the effects brought by different radius parameters. Again, fixing other parameters, we repeat our calculations by scaling the radius parameters

Proton partial waves					
L	J	$\lvert\mathbf{S}\rvert^2(\bar{V}{=}1.5)$	$\lvert\mathbf{S}\rvert^2(\bar{V}{=}1.0)$	$\lvert\mathbf{S}\rvert^2(\bar{V}{=}0.5)$	$\lvert\mathbf{S}\rvert^2(\bar{V}{=}0.0)$
0	0.5	6.45E-04	2.33E-04	1.56E-02	1.0
1	0.5	9.17E-04	1.17E-03	1.63E-02	1.0
2	1.5	8.33E-04	1.28E-04	1.34E-02	1.0
1	1.5	9.19E-04	1.23E-03	1.74E-02	1.0
2	2.5	7.97E-04	1.17E-04	1.52E-02	1.0
3	2.5	1.27E-03	1.64E-03	1.81E-02	1.0
4	3.5	1.51E-03	2.89E-04	1.02E-02	1.0
3	3.5	1.27E-03	1.85E-03	2.11E-02	1.0
...	...	...	...	...	...

Table 1: The modules of S-matrix for proton partial waves with varying imaginary potentials, where $\bar{V}$ is the scaled depth defined as $V_i(new)/V_i(initial)$.

Neutron partial waves					
L	J	$\lvert\mathbf{S}\rvert^2(\bar{V}{=}1.5)$	$\lvert\mathbf{S}\rvert^2(\bar{V}{=}1.0)$	$\lvert\mathbf{S}\rvert^2(\bar{V}{=}0.5)$	$\lvert\mathbf{S}\rvert^2(\bar{V}{=}0.0)$
0	0.5	7.88E-04	1.40E-03	2.16E-02	1
1	0.5	5.24E-04	4.68E-05	1.75E-02	1
2	1.5	8.94E-04	1.62E-03	2.29E-02	1
1	1.5	5.24E-04	4.68E-05	1.75E-02	1
2	2.5	8.94E-04	1.62E-03	2.29E-02	1
3	2.5	7.27E-04	1.66E-05	1.67E-02	1
4	3.5	1.15E-03	1.87E-03	2.51E-02	1
3	3.5	7.27E-04	1.66E-05	1.67E-02	1
...	...	...	...	...	...

Table 2: The modules of S-matrix for neutron partial waves with varying imaginary potentials, where $\bar{V}$ is the scaled depth defined as $V_i(new)/V_i(initial)$.

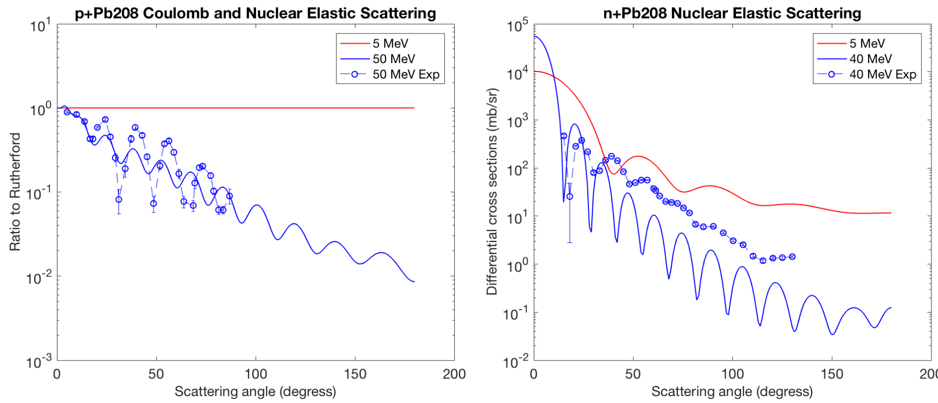

Figure 1: Differential cross sections for nucleons scattering with ^{208}Pb at 5 and 50MeV. Left panel is proton and right panel is neutron

r (including volume, surface derivative and spin-orbit potentials) a factor of 0.2, 0.5, 2, 3 and 4. The results are shown in Figure 2. For the proton, we observe the dramatic up-down shifts and denser diffraction patterns with increasing r. It's the synergistic effect by the Coulomb and optical potentials. As for neutron, the changing of pattern is relative small as it only feels the optical potential.

The total reaction cross section and the absorptive cross section are equal in a elastic scattering. For neutron, we extract them according to the equation

$$\sigma_e = \frac{\pi}{k^2} \sum_J (2J+1)(1-|\mathbf{S}_J|^2). \tag{6}$$

The total reaction and absorptive cross sections are 3.764×10^3 mb. The number deviates little from the value 3.796×10^3 mb given directly by FRESCO for slightly different physical constants used.

2 Fit optical potentials for elastic scattering of a nucleon on ^{208}Pb target

In this section we will do χ^2 data fitting to obtain optical potentials for the elastic scattering of a proton or neutron on ^{208}Pb. Experimental data are taken from Ref. [5] for proton and and [6] for neutron. The beam energies of proton and neutron are 49.35 MeV and 40.0 MeV, respectively. In addition, we choose the optical parameters employed in Sec. 1 (Ref. [3, 4]) as the starting point of our fitting. All the results discussed in this section are generated by SFRESCO (Ref. [2]).

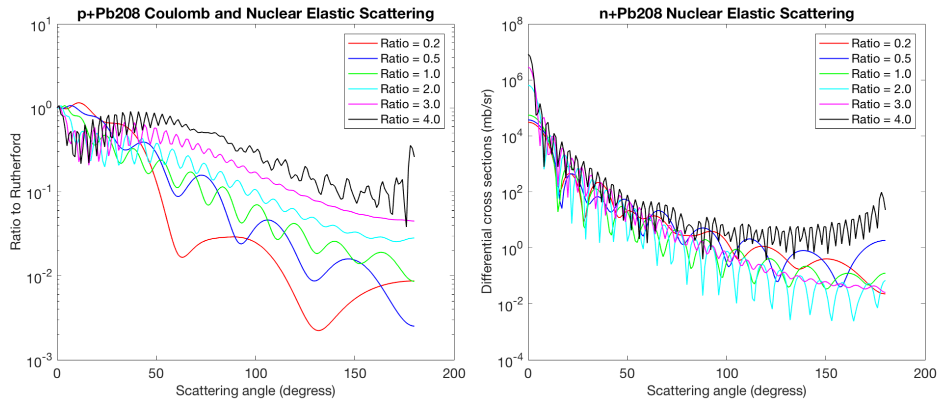

Figure 2: Differential cross sections for nucleons scattering with ^{208}Pb with different radius parameters at 50MeV, where ratio is defined as $r_{new}/r_{initial}$. Left panel is proton and right panel is neutron.

2.1 Fit process and results

All the intermediate and final results of our fitting are summarized in Table 3 (for proton) and Table 4 (for neutron). For simplicity, we neglect spin-orbit components at the beginning, and only volume real and volume imaginary components are included. Keeping the volume imaginary component unchanged, we fit the volume real part (index 2 in Table 3 and 4), which cannot reduce χ^2/N to a low value. Then, we vary both volume real and imaginary parts simultaneously (index 3 in Table 3 and 4) and achieve a significant improvement. However, for proton the diffuseness parameter av becomes too small to be considered physical.

Another choice of optical potential is to use a surface imaginary component instead of a volume one. Starting from parametrization of index 4 in Table 3 and 4, we fit the volume real part and surface imaginary part (index 5 in Table 3 and 4). For both proton and neutron, a surface imaginary component gives a lower χ^2/N, and thus we will add spin-orbit terms onto this optical potential form.

As shown in the last four lines in Table 3 and 4, we gradually add and fit different parameters in the spin-orbit term. As for proton, the description can hardly be improved by only adding a real spin-orbit potential (index 6 in Table 3). If we only add a imaginary spin-orbit component, the diffuseness parameter "awso" will become negative and thus unphysical (index 8 in Table 3), so we abandon this set of parameters. If both real and imaginary components of spin-orbit potential are included, χ^2/N will slightly decrease from 4.860 to 3.611, (index 9 in Table 3), which indicates that the spin-orbit term is not very important for the description of elastic scattering of a proton on ^{208}Pb.

As for neutron, the radius parameter "rvso" will become negative and unphysical when only a real spin-orbit component is included (index 6 in Table 4), so we abandon this set of parameters. By only adding an imaginary spin-orbit component, χ^2/N is slightly lowered from 4.638 to 3.310 (index 8 in Table 4). When both real and imaginary spin-orbit parts are varied, χ^2/N can be even lower (index 9 in Table 4). However, in this case the diffuseness “avso” will become less than radius “rvso”, which is unphysical and unacceptable. As no significant improvement is seen from adding spin-orbit term, we conclude that the spin-orbit term is not very important for the description of elastic scattering of a neutron on ^{208}Pb.

2.2 Sensitivity of final parameters to the initialization

Still empty.

Table 3: Fitting results of scattering of a proton on ^{208}Pb. The unit of Vv, Wv, Ws, Vso and Wso is MeV, and the unit of rv, av, rwv, awv, rws, aws, rvso, avso, rwso and awso is fm. Unphysical values are highlighted in red.

Index	Fit from	Vv	rv	av	Wv	rwv	awv	Ws	rws	aws	Vso	rvso	avso	Wso	rwso	awso	χ^2/N
1	-	67.2	1.244	0.646	16.6	1.244	0.646	-	-	-	-	-	-	-	-	-	78.285
2	1	46.1	1.262	0.574	16.6	1.244	0.646	-	-	-	-	-	-	-	-	-	27.134
3	2	44.6	1.254	1.87E-04	4.89	1.726	0.171	-	-	-	-	-	-	-	-	-	5.479
4	-	46.1	1.262	0.574	-	-	-	19.5	1.246	0.615	-	-	-	-	-	-	11.335
5	4	45.3	1.229	0.528	-	-	-	13.2	1.295	0.713	-	-	-	-	-	-	4.860
6	5	45.2	1.232	0.489	-	-	-	12.7	1.295	0.732	0.14	1.07	0.55	-	-	-	4.838
7	-	45.2	1.232	0.489	-	-	-	12.7	1.295	0.732	-	-	-	-3.1	1.08	0.57	12.026
8	7	45.1	1.242	0.507	-	-	-	12.0	1.279	0.748	-	-	-	-2.1	0.66	-0.028	4.068
9	7	45.2	1.276	0.540	-	-	-	15.7	1.239	0.710	-6.9	0.84	0.55	-8.0	1.03	0.53	3.661

Table 4: Fitting results of scattering of a neutron on ^{208}Pb. The unit of Vv, Wv, Ws, Vso and Wso is MeV, and the unit of rv, av, rwv, awv, rws, aws, rvso, avso, rwso and awso is fm. Unphysical values are highlighted in red.

index	Fit from	Vv	rv	av	Wv	rwv	awv	Ws	rws	aws	Vso	rvso	avso	Wso	rwso	aso	χ^2/N
1	-	50.6	1.244	0.646	15.6	1.244	0.646	-	-	-	-	-	-	-	-	-	261.394
2	1	40.3	1.245	0.903	15.6	1.244	0.646	-	-	-	-	-	-	-	-	-	46.553
3	2	41.9	1.154	0.762	6.598	1.383	0.824	-	-	-	-	-	-	-	-	-	7.900
4	-	40.3	1.245	0.903	-	-	-	13.8	1.246	0.510	-	-	-	-	-	-	98.423
5	4	36.4	1.269	0.585	-	-	-	14.4	1.097	0.500	-	-	-	-	-	-	4.638
6	5	36.1	1.277	0.578	-	-	-	15.7	1.108	0.498	8.3	-4.3	3.2	-	-	-	3.084
7	-	36.4	1.269	0.585	-	-	-	14.4	1.097	0.500	-	-	-	-3.1	1.08	0.57	35.163
8	7	36.4	1.273	0.593	-	-	-	15.2	1.109	0.519	-	-	-	-3.1	1.09	0.43	3.310
9	8	35.8	1.266	0.592	-	-	-	14.9	1.107	0.513	4.9	1.03	1.23	-3.0	1.06	0.81	2.258

References

[1] Ian J Thompson and Filomena M Nunes. Nuclear reactions for astrophysics: principles, calculation and applications of low-energy reactions. pages 62–64,129–131, 2009.

[2] I.J. Thompson. Fresco, coupled reaction channels calculations. `http://www.fresco.org.uk/`. Accessed Feb 25, 2018.

[3] Roberto Capote, Michel Herman, P Obložinskỳ, PG Young, Stéphane Goriely, T Belgya, AV Ignatyuk, Arjan J Koning, Stéphane Hilaire, Vladimir A Plujko, et al. RIPL–reference input parameter library for calculation of nuclear reactions and nuclear data evaluations. *Nuclear Data Sheets*, 110(12):3107–3214, 2009.

[4] AJ Koning and JP Delaroche. Local and global nucleon optical models from 1 keV to 200 MeV. *Nuclear Physics A*, 713(3-4):231–310, 2003.

[5] G.S. Mani, D.T. Jones, and D. Jacques. Elastic scattering of 50 MeV protons by nuclei in the range from ^{42}Ca to ^{208}Pb. *Nuclear Physics A*, 165(2):384 – 392, 1971.

[6] R. P. DeVito, Dao T. Khoa, Sam M. Austin, U. E. P. Berg, and Bui Minh Loc. Neutron scattering from ^{208}Pb at 30.4 and 40.0 MeV and isospin dependence of the nucleon optical potential. *Phys. Rev. C*, 85:024619, Feb 2012.